G-quadruplex DNA drives genomic instability and represents a targetable molecular abnormality in ATRX-deficient malignant glioma

Yuxiang Wang[1], Jie Yang[2], Wei Wu[1], Rachna Shah[1], Carla Danussi[3], Gregory J. Riggins[4], Kasthuri Kannan[5], Erik P. Sulman[2,6], Timothy A. Chan[1,7], and Jason T. Huse[3,6]*

[1]Human Oncology and Pathogenesis Program and [7]Department of Radiation Oncology, Memorial Sloan-Kettering Cancer Center, New York, NY 10065

Departments of [2]Radation Oncology, [6]Pathology, and [3]Translational Molecular Pathology, University of Texas MD Anderson Cancer Center, Houston, TX 77030

[4]Departments of Neurosurgery, Oncology, and Genetic Medicine, Johns Hopkins School of Medicine, Baltimore, MD 21231

[5]Department of Pathology, New York University School of Medicine, New York, NY 10016

* To whom correspondence should be addressed: 2130 W Holcombe Blvd, LSP 9.4009, Unit 2951, Houston, TX 77030; ph.: 713-745-3186; Email: jhuse@mdanderson.org

Key words: glioma, ATRX, G-quadruplex, G4, DNA damage, synthetic lethality, cancer

Running Title: Targeting G-quadruplexes in ATRX-deficient glioma

Abstract: 138 words; Main text: 3306 words; Methods: 1616 words; 7 Figures; 5 Supplementary Figures; 2 Supplementary Tables; 64 references

Abstract

Mutational inactivation of *ATRX* (α-thalassemia mental retardation X-linked) represents a defining molecular alteration in large subsets of malignant glioma. Yet the pathogenic consequences of ATRX deficiency remain unclear, as do tractable mechanisms for its therapeutic targeting. Here we report that ATRX loss in isogenic glioma model systems induces replication stress and DNA damage by way of G-quadruplex (G4) DNA secondary structure. Moreover, these effects are associated with the acquisition of disease-relevant copy number alterations over time. We then demonstrate, both *in vitro* and *in vivo*, that ATRX deficiency selectively enhances DNA damage and cell death following chemical G4 stabilization. Finally, we show that G4 stabilization synergizes with other DNA-damaging therapies, including ionizing radiation, in the ATRX-deficient context. Our findings reveal novel pathogenic mechanisms driven by ATRX deficiency in glioma, while also pointing to tangible strategies for drug development.

Infiltrating gliomas are the most common primary brain tumors and, despite considerable molecular and clinical heterogeneity, remain uniformly deadly in the face of aggressive surgical and cytotoxic treatment regimens[1]. Recent large-scale genomic profiling has shown that inactivating mutations in *ATRX* (α-thalassemia mental retardation X-linked) characterize large subclasses of both adult and pediatric glioma[2-4]. Despite these striking correlations, however, the precise mechanisms by which *ATRX* mutation promotes gliomagenesis remain unclear. Indeed, germline mutations in *ATRX* do not predispose affected individuals to cancer, causing instead a rare, congenital neurodevelopmental condition associated with intellectual disability (ATR-X syndrome)[5]. *ATRX* encodes a chromatin binding protein widely implicated in epigenetic regulation and remodeling[6-12], suggesting that epigenomic dysfunction may, at least in part, underlie the oncogenic effects of ATRX deficiency. *ATRX* loss has also been implicated in alternative lengthening of telomeres (ALT), an abnormal telomerase-independent mechanism of telomere maintenance based on homologous recombination[13,14]. Finally, ATRX deficiency has been repeatedly linked to replication stress, DNA damage, copy number aberrations, and aneuploidy[15-20]. Whether and how such genomic instability contributes to the initiation or evolution of malignant glioma remains unclear.

ATRX binds widely across the genome at sites featuring tandem repeats and CpG islands[21]. Many such loci are GC-rich and susceptible to forming G-quadruplexes (G4s), abnormal secondary structures implicated in both transcriptional dysregulation and DNA damage. Accordingly, it has been hypothesized that, among its various functionalities, ATRX serves to resolve G4s genome-wide and mitigate their deleterious consequences[21,22]. The tendency of G4s to stall replication forks underlies their association with DNA damage[23]. Chemical stabilization of G4s induces replication stress at genomic loci prone to G4 formation[24], and also promotes DNA damage and apoptosis in neural progenitor cells[25]. Moreover, recent work suggests that G4-induced

replication stress at telomeres may drive ALT in the ATRX-deficient setting through induction of homologous recombination[13]. Indeed, G4 stabilization hampers the ability of forced ATRX expression to abrogate the ALT phenotype *in vitro*. Taken together, these findings provide compelling links between ATRX, G4 biology, and genomic instability. Whether ATRX deficiency directly induces G4 formation and DNA damage, however, remains unestablished, as does the impact of G4s on the pathogenesis of ATRX-deficient neoplasia. Moreover, therapeutic strategies leveraging G4 biology in the selective targeting of ATRX-deficient cancers have not been extensively explored.

To characterize the role of G4-mediated genomic instability in glioma biology, we reversibly inactivated ATRX in an isogenic normal human astrocyte (NHA) model. We found that ATRX loss increased G4 formation, replication stress, and DNA damage genome-wide. Moreover, ATRX-deficient NHA's accumulated clinically relevant copy number aberrations (CNAs) at an accelerated rate relative to ATRX-intact counterparts. Chemical G4 stabilization was associated with enhanced DNA damage and cell death in ATRX-deficient context. Moreover, ATRX-mutant glioma stem cell (GSC) xenografts were selectively sensitive to G4 targeting *in vivo*. Finally, G4 stabilization in ATRX-deficient cells effectively synergized with other DNA-damaging treatment strategies, including ionizing radiation. These findings clarify distinct mechanisms by which G4s influence ATRX-deficient glioma pathogenesis and indicate that G4-stabilization may represent and attractive therapeutic strategy for the selective targeting of ATRX-mutant cancers.

Results

ATRX deficiency promotes G4 formation, DNA damage, and chromosome breaks. To model the genomic consequences of ATRX deficiency in a glioma-relevant cellular context, we performed shRNA-mediated ATRX knockdown in TERT and E6/E7-

transformed normal human astrocytes (NHAs). Several studies have effectively employed immortalized NHAs to delineate key aspects of glioma biology [26-30]. In our investigations, we employed two distinct hairpin constructs to silence *ATRX*—shATRX1 and shATRX2—the latter of which was driven by a doxycycline (dox)-inducible promoter (FIG. 1a). This framework allowed for the analysis of both immediate and long-term effects of ATRX deficiency as well as their reversibility. Using a monoclonal antibody known to recognize G4 structures *in situ* (1H6), we then demonstrated that ATRX deficiency increased nuclear G4s relative to levels seen in control shRNA-expressing parental NHAs (shCon), an effect that was reversible upon restored ATRX expression (FIG. 1b-1c). Increased G4s were also found in murine neuroepithelial progenitor cells featuring inactivated *Atrx* (Supplementary FIG. 1a). The specificity of 1H6 for DNA-based secondary structures was confirmed by DNAase treatment, which eradicated immunolabelling, and RNase treatment, which did not, in NHAs treated with the G4 stabilizing agent CX-3543 (see below, Supplementary FIG. 1b). We also employed a synthetic single-chain antibody (hf2) to immunoprecipitate G4s in both ATRX-intact and ATRX-deficient contexts. hf2 specificity was validated by gel-shift assay showing specific capture of synthesized Kit2 nucleotides independently from random ssDNA and dsDNA (Supplementary FIG. 1c). We then performed pulldowns in our isogenic NHAs, finding that ATRX deficiency significantly increased the qPCR enrichment of known G4 sites within the MYC and ZNF618 loci, as well as in telomeric regions on chromosomes 1, 2, and X (FIG. 1d)[31-33]. Consistent with the notion that ATRX resolves G4s as part of its normal functionality, we found a distinct absence of colocalization between ATRX and G4 immunofluorescence in ATRX-intact NHAs (FIG. 1e). Finally, functional studies demonstrated that ATRX knockdown failed to induce significant changes in apoptosis, BrdU incorporation, or cell cycle profile (Supplementary FIG. 1d-1f). Taken together, these findings confirm, in a true isogenic system, that ATRX deficiency promotes G4

formation. Moreover, they indicate that, at least in this glioma-relevant context, increased G4s as a consequence of ATRX deficiency are insufficient to drive apoptosis or impact cellular proliferation.

We then examined whether the G4s induced by ATRX deficiency promoted replication stress and DNA damage, as suggested by prior literature[34]. We found that ATRX knockdown significantly increased γ-H2AX-positive foci by immunofluorescence (FIG. 2a-2b), and did so in a pattern the extensively colocalized with nuclear G4 distribution (FIG. 2c). Moreover, these changes were accompanied by engagement of the replication stress pathway, as evidenced by upregulated levels p-CHK1 and p-KAP1 on Western blot (FIG. 2d). To determine whether increased levels of DNA damage in the ATRX-deficient setting might lead to structural abnormalities in chromosomes, we performed metaphase cytogenetic analysis coupled with telomere-fluorescence in situ hybridization (FISH) in Par-Con and ATRX-deficient NHAs uniformly aged to 15 passages. Consistent with multiple prior reports, ATRX knockdown in this context was not associated with an obvious ALT phenotype (Supplementary Figure 2a-2b). However, we consistently observed increased numbers of chromosome breaks in ATRX-deficient NHAs relative to shCon counterparts (FIG. 2e and Supplementary FIG. 2b). These data establish pathogenic links between G4s arising with ATRX deficiency and the generalized genomic instability characteristic of ATRX-mutant tumors and cell lines.

ATRX deficiency drives clinically relevant CNA formation. Having confirmed that ATRX deficiency induces DNA damage and structural abnormalities in chromosomes, likely through G4-mediated mechanisms, we sought to assess whether these biological processes might promote acquisition of CNAs in ATRX-deficient tumors. *ATRX* mutations in adult glioma arise almost exclusively in the setting of concurrent mutations in *TP53* and either *IDH1* or *IDH2*. The glioma subclass defined by this combined genotype, termed “IDHmut-noncodel” [2], features almost uniformly low-level

144 *ATRX* expression and exhibits a characteristic pattern of CNAs, distinct form that
145 commonly seen in other adult disease subclasses (Supplementary FIG. 3). Moreover,
146 multiple CNAs recurrently featured in ATRX-deficient glioma mobilize established
147 oncogenic and/or tumor suppressive loci, including *MYC* and *CDKN2A*[2], implying that
148 such structural abnormalities may contribute to the malignant evolution of this inexorably
149 progressive cancer.

150 To experimentally model CNA formation in the ATRX-deficient setting, we aged
151 our isogenic NHAs in culture, monitoring DNA copy number by SNP array at 5 and 15
152 passages—~1 month and ~3 months in culture, respectively (Supplementary FIG. 3).
153 We found that while both sets of isogenics demonstrated increased CNAs over time,
154 ATRX-deficient NHAs exhibited a distinct pattern of gains and losses that included larger
155 (> 1 Mb) alterations not seen ATRX-intact counterparts (FIG. 3a). Analysis of TCGA
156 SNP data revealed a similar subset of broad alterations included within the CNA profile
157 of IDHmut-noncodel gliomas (FIG. 3b). Moreover, two of the broad CNAs associated
158 with ATRX deficiency *in vitro*, involving 12p gain and 14q loss, recapitulated events
159 commonly seen in the IDHmut-noncodel glioma subclass and associated with relatively
160 unfavorable prognosis when present (FIG. 3c-3f). Taken together, these findings
161 support the notion that G4-mediated DNA damage induces specific types and patterns of
162 CNAs in ATRX-deficient glioma, which in turn influence the malignant evolution of the
163 disease.

164 ***Chemical G4 stabilization selectively targets ATRX-deficient NHAs and***
165 ***enhances their sensitivity to ionizing radiation.*** As indicated above, the pronounced
166 effects of ATRX deficiency on G4 formation and replication stress in NHAs were not
167 associated with increased cell death a baseline. Nevertheless, we reasoned that
168 compensatory mechanisms to resolve G4s and otherwise maintain genomic integrity
169 were likely under increased stress, and that chemical stabilization of G4s might,

therefore, selectively enhance DNA damage to an unsustainable degree in the ATRX-deficient context. To evaluate the therapeutic potential of this synthetic lethal approach, we treated our isogenic NHAs in culture with increasing concentrations of CX-3543 (Quarfloxin), an established G4-stabilizing agent[35,36]. We found that ATRX knockdown, in both constitutive and inducible systems, was associated with increased sensitivity to CX-3543 (IC50 = 42.449 nM (shATRX1) vs 328.835 nM (shCon) in constitutive NHAs and IC50 = 357.424 nM (pre-induction) vs 53.415 nM (shATRX2) vs 247.700 nM (post-induction); FIG. 4a-4b). Clonogenicity studies revealed similarly enhanced vulnerability to CX-3543 in ATRX-deficient NHAs as well as normally ATRX-intact GSCs (TS 543) subjected to ATRX knockdown (FIG. 4c-4d). Restoring ATRX expression reverted NHAs to baseline levels of sensitivity (FIG. 4b).

γ-H2AX immunofluorescence demonstrated dramatically increased levels of DNA damage in ATRX-deficient NHAs treated with CX-3543, accompanied by activation of the replication stress pathway as determined by western blot (FIG. 4e-4h). Moreover, 53BP1-positive foci of DNA damage demonstrated extensive co-localization with G4s by immunofluorescence on confocal microscopy (Supplementary FIG. 4). Once again, these effects were reversed following ATRX re-expression (FIG. 4f, 4h). Annexin V flow cytometry confirmed that the heightened sensitivity of ATRX-deficient NHAs to CX-3543 reflected increased apoptosis, and this enhanced cell death followed the kinetics of replication stress pathway activation in both constitutive and inducible isogenic contexts (FIG. 5a-5d). In total, these results indicate that chemical stabilization of G4 structures selectively promotes cell death in the ATRX-deficient context, likely by inducing toxic levels of DNA damage.

The experimental links, described above, between replication stress, DNA damage, and CX-3543 treatment prompted us to consider whether G4 stabilization might enhance the therapeutic efficacy of established DNA-damaging treatment strategies,

196 particularly in ATRX-deficient setting. To evaluate this possibility, we subjected vehicle
197 and CX-3543-treated isogenic NHAs, cultured in soft agar, to increasing doses of either
198 ionizing radiation (IR) or hydroxyurea (HU), assessing viable colonies at 21 days. We
199 found that CX-3543 treatment potentiated the cytotoxicity of both IR and HU, and while
200 these effects were significant for all cellular genotypes, they were particularly strong in
201 ATRX-deficient NHAs (FIG. 5e-5f). Moreover, restoring ATRX expression markedly
202 dampened the extent of cytotoxic synergy. These findings inform additional
203 therapeutically relevant strategies combining chemical G4 stabilization with well-
204 established treatment modalities in the targeting of ATRX-deficient cancer.
205 ***ATRX deficiency enhances sensitivity to chemical G4 stabilization in vivo***.
206 Having established the increased sensitivity of ATRX-deficient NHAs and GSCs to
207 chemical G4 stabilization in cell culture, we sought to ascertain whether this approach
208 could exhibit a similar degree of efficacy *in vivo*. To this end, we employed an *ATRX*-
209 mutant, patient-derived GSC line (JHH-273) capable of forming tumors in murine hosts
210 when embedded in the hind flank[37]. Following cellular implantation, we subjected
211 xenografted mice to daily intravenous treatment with either CX-3543 or vehicle and
212 monitored tumor growth over time. We found that CX-3543 dramatically slowed the
213 growth of JHH-273 flank tumors (FIG. 6a-6b and Supplementary FIG. 5a) and
214 significantly prolonged survival xenografted mice (FIG. 6c). Histopathological
215 examination of CX-3543-treated xenografts revealed cellular depopulation, reduced
216 proliferative activity by Ki-67 immunostaining, and increased γ-H2AX-positive DNA
217 damage foci relative to untreated counterparts, recapitulating *in vitro* findings (FIG. 6d).
218 Notably, telomere FISH failed to reveal changes in the level of ALT in residual viable
219 tumor following CX-3543 treatment (FIG. 6d). To ascertain whether these effects were
220 specific to the *ATRX*-mutant context, we performed analogous xenograft experiments
221 using *ATRX*-wild type TS 543 cells. In these studies, we found that CX-3543 treatment

had no appreciable effect on either xenograft growth or mouse survival (FIG. 7a-7b and Supplementary FIG. 5b). However, when we subjected these same GSCs to ATRX knockdown, they were rendered sensitive to CX-3543 to an extent similar to that observed for JHH-273 cells (FIG. 7c-7d and Supplementary FIG. 5c). ATRX knockdown also recapitulated histopathological effects on cellular depopulation, proliferative activity, and γ-H2AX-positivity (FIG. 7e-7f). Consistent with prior reports[16,19], ATRX knockdown was not associated with ALT in TS 543 cells (Supplementary FIG. 7e-7f). Taken together, these *in vivo* findings further support the therapeutic potential for chemical G4 stabilization in the selective targeting of ATRX-deficient glioma.

Discussion

As indicated above, loss-of-function mutations in *ATRX* likely play central pathogenic roles in several distinct tumor variants, including multiple subtypes of incurable glioma. That *ATRX* itself encodes a chromatin regulatory protein suggests that epigenomic dysfunction underlies, at least in part, the oncogenic sequelae of its inactivation. To this point, we recently demonstrated that ATRX deficiency induces extensive chromatin remodeling and transcriptional shifts in putative glioma cells of origin, driving disease-relevant phenotypes that modulate both cellular motility and differentiation[38].However, the full impact of ATRX deficiency on tumor initiation and evolution almost certainly includes other molecular mechanisms. The association of *ATRX* mutation and ALT[14,19], for instance, is now extensively described and provides a vehicle to telomerase-independent immortalization in affected cancer cells. Moreover, recent work has linked ALT to the well-characterized genomic instability induced by ATRX deficiency[13,39].

The pathogenic consequences of ATRX-dependent genomic instability in the context of cancer are unknown. Abundant prior work has demonstrated links between

ATRX deficiency, DNA damage, CNA development, and aneuploidy[15-20]. Indeed, p53-dependent apoptosis derived from genomic instability in the neuroepithelial progenitor compartment likely underlies the neuronal depopulation, microcephaly, and mental retardation associated with ATR-X syndrome[40]. Replication stress has been extensively implicated as a root cause of genomic instability in ATRX-deficient cells[16,18,41]. In addition to activating DNA damage pathway signaling, replication fork stalling and collapse can generate double-strand breaks and defective chromosome condensation during mitosis, both of which are known to drive CNAs and aneuploidy of the kind seen in *ATRX*-mutant glioma[42-44]. Recent work strongly supports the notion that the replication stress characterizing ATRX-deficient cells derives, at least in part, from G4 DNA secondary structure[13,23-25]. ATRX binds widely at GC-rich genomic sites susceptible to forming G4s[21], and restored ATRX expression in *ATRX*-mutant cell lines mitigates G4-associated phenotypes such as ALT[13]. Such data implies that ATRX may serve to protect the genome from unwanted G4 formation and the potentially deleterious consequences of ensuant genomic instability. Our findings support this conjecture by demonstrating, for the first time, that ATRX deficiency potently and reversibly induces G4 formation in an isogenic experimental context. As such, they confirm a novel functionality for a SWI/SNF epigenetic regulator already widely implicated in chromatin remodeling, structure, and organization.

That increased G4s were accompanied by replication stress signaling, DNA damage at spatially overlapping sites, and disease-relevant patterns of CNAs in our cell line models provides additional evidence that this pathobiological cascade features in ATRX-mutant neoplasia. Prior computational analysis across multiple tumor types established significant correlations between CNA breakpoints and genomic sites enriched in putative G4-forming sequences[45], firmly implicating G4s in the process of cancer-associated CNA acquisition. In our NHA models, ATRX knockdown led to a

distinct CNA profile over time enriched in alterations over 1 Mb in size. While this pattern did not completely mirror the known CNA signature of *ATRX*-mutant gliomas[2], it did recapitulate key elements involving larger, arm-level events. In particular, two CNAs (12p gain and 14q loss) were reminiscent of analogous alterations in human tumors associated with unfavorable prognosis. These data speak directly to the premise that CNA mobilization, driven at least in part by G4-mediated DNA damage, promotes malignant evolution in ATRX-deficient gliomas. As this tumor subtype characteristically progresses slowly over time[46], such mechanistic insights are consistent with established clinical features.

Due to its sheer prevalence in glioma, ATRX deficiency represents a molecular target of intriguing therapeutic potential. That being said, effective strategies to drug an inactivated epigenetic regulator are not immediately obvious, as they might be in the setting of more conventional, kinase-predominant, oncogenic signaling networks. Given these challenges, leveraging specific vulnerabilities engendered by ATRX loss might offer alternative approaches. In particular, the longstanding association of ATRX deficiency with genomic instability, confirmed in this report, presents a tangible opportunity to explore a synthetic lethality paradigm, akin to that of Poly (ADP-ribose) polymerase (PARP) inhibitors in the treatment of *BRCA1*-inactivated breast cancer[47]. While the observed level of DNA damage in our ATRX-deficient cell line and tumor models was insufficient to induce apoptosis in isolation, due in part to coincident *TP53* inactivation, we hypothesized that its targeted enhancement would overwhelm compensatory mechanisms maintaining cell viability. Moreover, our identification of G4s as the likely source of ATRX-deficient genomic instability provided a viable approach to therapeutic selectivity.

CX-3543 is an established G4 stabilizing agent that, despite limited bioavailability, has advanced to Phase II clinical trials in at least one instance[35]. In our studies, ATRX-

deficient cell lines and tumors exhibited selective sensitivity to CX-3543 *in vitro* and *in vivo*. Moreover, cell death in these contexts was temporally associated with DNA damage and replication stress, speaking to likely mechanism of action. We cannot completely exclude the possibility that CX-3543 exerts some of its cytotoxic effects though the manipulation of ALT. As alluded to above, prior work has functionally linked increased G4s and DNA damage at telomeres with ALT induction in ATRX-deficient cells[13]. Nevertheless, ATRX knockdown was not associated with ALT in our NHA and TS 543 isogenics, consistent with multiple prior reports[16,17,19], and CX-3543 failed to alter the pattern of telomere FISH in *ATRX*-mutant JHH-273 GSC xenografts. Taken together, these findings strongly suggest that the cytotoxicity of CX-3543 in the ATRX-deficient context is, at least in large part, mediated by increased DNA damage genome-wide, not limited to telomeric regions.

We also demonstrated that CX-3543 dramatically enhanced the effects of IR and HU in ATRX-deficient NHAs, highlighting possibilities for effective synergistic combinations in the clinical setting. Since its introduction almost 40 years ago, IR has remained one of the most important nonsurgical therapeutic modalities employed in the treatment of malignant glioma, with demonstrated efficacy across glioma subtypes[48-50]. Moreover, recent work has shown that ATRX-mutant gliomas in particular exhibit increased sensitivity to DNA-damaging combinations of IR and chemotherapy[51,52]. This vulnerability may derive in part from increased genomic instability at baseline. Defective non-homologous end joining (NHEJ), documented to arise with ATRX deficiency in preclinical models[17], may also play a role. Moreover, IDH mutations, which almost invariable co-occur with ATRX deficiency in adult glioma, are known to disable homologous recombination (HR)-mediated DNA repair[53-55]. Regardless of the precise molecular mechanisms at work, therapeutically potentiating an already effective

325 treatment strategy for glioma represents an underexplored approach with the potential
326 for considerable clinical impact.

327 Whether CX-3543 itself represents an optimal agent for clinical translation in
328 glioma remains unclear. Phase I trials were reportedly terminated due to poor
329 compound bioavailability[36], and no formal blood-brain barrier penetration studies have
330 been released. Nevertheless, our findings indicate that the targeted approach of G4-
331 stabilization has considerable therapeutic potential in the treatment of ATRX-deficient
332 glioma, along with other *ATRX*-mutant cancers. That the strategy is based on a tumor-
333 specific vulnerability arising in association with an easily assessable biomarker should
334 facilitate its clinical application, while also minimizing harmful side effects in treated
335 patients. Moreover, alternative G4 stabilizing agents with more favorable
336 pharmacokinetic profiles than CX-3543 are currently available for use both as tool
337 compounds and starting points for chemical derivatization[56,57].

338 In summary, we firmly implicate G4 secondary structure as a defining
339 characteristic of *ATRX*-mutant glioma, one that drives disease-relevant genomic
340 instability and presents opportunities for tangible therapeutic advancement. As such,
341 our work has important implications for both the molecular pathogenesis of ATRX-
342 deficient neoplasia as well as the development of more effective drugs specifically
343 targeting a palette of deadly tumors.

344

345 **Methods**

346 **Study design.** The objective of this study was to determine the impact of ATRX
347 deficiency on G4 formation, DNA damage, and genomic instability in glioma, and assess
348 the potential of chemical G4 stabilization as a therapeutic strategy in ATRX-deficient
349 tumors. This was a controlled, laboratory-based, experimental study using cell line
350 models in culture and in xenografts. ATRX was inactivated by genetic approaches and,

in some cases, pharmaceutical agents and/or ionizing radiation were applied. Sample sizes were determined independently for each experiment without formal power calculation. No data was excluded from analysis. Unless otherwise specified, experiments employed three replicates per sample. Endpoints varied by experiment and are described below, in figure legends, or in the Results section. Histopathological and immunohistochemical review of xenografts was conducted by a Neuropathologist (J.T.H.) in a nonblinded fashion. Quantification of G4 and/or γ-H2AX immunostaining in NHAs was blinded.

Cell culture and generation of ATRX-deficient cell lines. The parental immortalized normal human astrocyte line was a gift from R.O. Peiper (UCSF) [58]. TS 543 is a patient-derived glioma tumorsphere line harboring *PDGFRA* amplification [59] and maintained in NeuroCult™ NS-A Proliferation media (#05751, Stemcell). ATRX knockdown was achieved by introducing either a modified FUGW vector (a gift from David Baltimore (Addgene plasmid # 14883)) carrying an shRNA expression cassette against *ATRX* (shATRX1) (see Supplementary Table 1 for shRNA sequences), a TRIPZ TET-inducible vector (Dharmacon) containing a distinct shRNA against ATRX (shATRX2), or a third shRNA against ATRX (sh590) from the TRC shRNA library (Sigma). shATRX1 and shATRX2 positive cells were FACS-sorted every 2 passages by fluorescent marker (RFP) for the top 5% of total population to ensure high shRNA expression. Sh590 positive TS543 cells were subjected to puromycin-based selection.

Proliferation, cell cycle and apoptosis analyses. Flow-cytometry analyses of proliferation and cell cycle were performed using the BD Pharmingen BrdU Flow Kit (# 559619). Apoptosis assays were performed using the Dead Cell Apoptosis Kit (# V13241, Thermo Fisher) with Propidium Iodide (PI) substituted by DAPI to avoid RFP interference.

In Situ visualization of G-quadruplexes, γ-H2AX and 53BP1. The 1H6 antibody was a gift from Dr. Peter M. Lansdorp[60]. For immunostaining, cells were grown in chamber slides (Nunc Lab-Tek II, cat no. 154526, Thermo Fisher) and synchronized to G0 phase by 24-hour serum starvation. The cells were digested with 10mg/ml proteinase K for 1h at 37°C, followed by fixation (4% paraformaldehyde in PBS for 10 min) and permeabilization (0.5% Tween, 0.2% Triton X-100 in PBS, 10 min). To eliminate RNA-structures, cells were treated with 20 ug/500 ul RNase A (Invitrogen). To confirm specificity towards DNA-G4, cells were incubated in 40mM Tris Cl (pH 8), 5mM CaCl2, 2mM MgCl2, 100 ug/ml BSA alone or including 0.06 U/ul of DNase I (Promega) and 80 gel units/ul of micrococcal nuclease (#M0247S, New England Biolabs) at 37°C for 2h. For staining, cells were blocked with goat serum (Sigma) for 4h at room temperature, then incubated with 0.5 ug/ml 1H6 antibody at 4°C overnight. Slides were then washed 5 times with PBST, incubated with Alexa Fluor 488 or 568 goat anti-mouse IgG (Invitrogen) at room temperature for 2 h, washed 5 times with PBST and mounted with coverslips using ProLong Gold antifade reagent and DAPI counterstain (Invitrogen). For γ-H2AX monostaining or 53BP1/G4 double staining, cells were treated with or without 100 nM CX-3543 for 3 days prior to synchronization to G0, and stained with γ-H2AX antibody (# 05-636, Millipore), or 53BP antibody (cat# NB100-304, Novus Biologicals) together with the 1H6 G4 antibody.

G4 pulldowns. Plasmid expressing hf2 was a kind gift of Dr. Shankar Balasubramanian[61]. Hf2 antibodies were expressed in Bl21 competent cells and purified with Protein A Sepharose (#P9424, Sigma) as previously described[62]. For G4 pulldowns, 2 µg of hf2 and 50 µl of Protein A Dynabeads (#10001D, ThermoFisher) were mixed and incubated overnight rotating at 4°C. Beads were washed with PBS for 5 times. 10 µg of genomic DNA from NHAs was sonicated and incubated with beads in 0.5% BSA overnight rotating at 4°C, followed by 6 washes with 10 mM Tris pH 7.4, 100 mM KCl,

0.1 % tween and one wash with 10 mM Tris pH 7.4, 100 mM KCl. Bound DNA was eluted in 50 µL of 1% SDS, 0.1 M NaHCO3 at 30 °C for one hour then purified by QIAquick PCR Purification Kit (Qiagen) to a final volume of 20 µL. The recovered DNA was used to determine enrichment of telomeric sequence (Tel1, 2 and X) and the promoter regions of *MYC* and *ZNF618*, using the *ESR1* promoter as a negative control (See Supplementary Table 2 for primer sequences).

TEL-FISH and metaphase cytogenetic analysis. For cell lines, resuspended cells were incubated with Colcemid (0.1 µg/ml) at 37 °C for 45 min, resuspended in 0.075 M KCl and incubated at 37 °C for 10 min, followed by fixation in methanol:acetic acid (3:1) solution. TEL-FISH was performed according to standard procedures using a CY3-conjugated, telomere-specific nucleic acid probe: 5'-TTAGGGTTAGGGTTAGGG-3' (Applied Biosystems). For xenograft tissues, tumors were removed and subjected to OCT embedding followed by 5 µm sectioning. Frozen sections were fixed with 4% paraformaldehyde for 10 min. After denaturing at 85 °C for 5 minutes in 10 mM Tris-HCL pH 7.2, 70% formamide, 0.5% blocking solution reagent (Roche), hybridization was performed as described above.

Cell viability and clonogenic assay. For standard viability assays, cells (500 cells/well) were incubated with a serial concentration of CX-3543 (10-300nM) for 7 days in 96-well plates. Cell viability was then assessed with the CellTiter-Glo Luminescent Assay (Promega) according to manufacturer-recommended procedures. To determine clonogenic ability, NHA or TS 543 cells were seeded at 5,000 cells/10-cm dish and incubated with vehicle or 50 nM CX-3543 for 14 days. Cells were fixed with 4% paraformaldehyde and stained with 0.005% crystal violet in PBS, followed by 3 washes in PBS and 2 washes in ddH_2O. For soft agar colony formation assays, 50,000 cells were seeded in 6-well plates containing 1% bottom layer and 0.5% top layer soft agar. Cells were then cultured in growth media with or without 50 nM CX-3543. Radiation

dosing of 0, 1, 2 or 4 Gy was immediately applied after plating. The 1.5 ml growth media covering the agar cultures was replenished every week. At day 21, colonies were fixed with 4% paraformaldehyde for 30 min and stained with 0.005% crystal violet in PBS overnight. Stained colonies were then washed extensively in PBS and water, and quantified on a Gelcount colony counter (Oxford Optronix).

SNP arrays. Genomic DNA was isolated from ATRX-deficient NHAs at passages 5 and 15. As controls, genomic DNA from ATRX-intact parental NHAs was derived at the start point (P0), P5 and P15. Extracted DNA was subjected to Affymetrix Genome-Wide Human SNP 6.0 array analysis(cat# 901182, ThermoFisher) according to the manufacturer's protocol. Preliminary copy number derivation and segmentation was conducted as previously described [63,64]to obtain CNV segment files with the following information: chromosome, start position, end position, probe number, and segment mean value. For analysis, we focused variations with absolute segment mean value > 0.5 for LGG samples and > 0.1 for NHA lines. All variations associated with ChrX and ChrY were excluded. CNV length was calculated by using the end position minus the start position. Data were visualized using IGV and GISTIC2.0.

Xenograft experiments. All animal protocols and procedures were performed in the xenograft suite at Memorial Sloan-Kettering Cancer Center in accordance with Institutional Animal Care and Use Committee (IACUC) guidelines. JHH-273 samples were kind gifts from Dr. Gregory Riggins at the Johns Hopkins University. Tumor samples were mechanically dissociated and small pieces (0.2 mm^3/flank) were embedded into the flanks of nude mice (Taconic Farms). In parallel, ATRX-intact and ATRX-deficient TS 543 cells at exponential growth phase were dissociated with Accutase (#07920, Stemcell), resuspended in Neurocult media, mixed with Matrigel (#356234, Corning) (1:1) and injected into nude mice flanks in a 50 ul mixture containing $5x10^6$ cells. Mice were randomized to vehicle or CX-3543 (12.5 mg/kg) treatment

groups. Drug delivery occurred via intravenous injection once per day, on a 5 day/week schedule until health-related defined end points. Tumor volumes were measured by calipers and calculated using the formula $(l \times w^2)/2$, where w is width and l is length in mm. For survival experiments, mice were treated until they reached health-related end points (2000 mm^3 tumor volume). For growth curve comparisons, all mice in a study cohort were sacrificed when the first mouse reached the 2000 mm^3 tumor size threshold. An independent cohort was used for Kaplan-Meier analysis. Xenografted tissues were removed, weighted and split into two parts. One part was snap frozen for TEL-FISH, while the other half was subjected to FFPE processing. 5µm FFPE sections were deparaffinized and subjected to antigen retrieval. Sections were blocked for non-specific binding with goat serum for 2h, followed by staining with Ki67 (5µg/ml, ab15580, Abcam) or γ-H2AX (1:1000, # 05-636, Millipore) antibodies at 4°C overnight. Sections were washed and incubated with secondary antibody. Ki67 staining were counterstained with Hematoxylin, and γ-H2AX staining were counterstained with DAPI.

Statistics. Unless otherwise stated, all results, representing at least three independent experiments, were plotted as mean ± SEM. In general, data were statistically analyzed using unpaired Student's *t* tests. Log-rank (Mantel-Cox) test were used to determine the significance of differences in Kaplan-Meier analysis of LGG patients and of hind flank xenograft experiments. 2-way ANOVA was used to compare the growth curves of xenografts and the colony formation assays. P values are represented using * for $P < 0.05$, ** for $P < 0.01$, *** for $P < 0.001$, and **** for $P < 0.0001$.

Data and materials availability. All data (raw and processed) and materials related to this manuscript will be made available upon request, utilizing material transfer agreements when appropriate.

Acknowledgments: We would like to thank Drs. Peter Lansdorp and Shankar Balasubarmanian for providing the 1H6 and hf2 antibodies, respectively. We would also like to acknowledge Dr. Cameron Brennan for providing the TS 543 GSC line. Finally, we would like to acknowledge the Genomics Core Facility at the Albert Einstein College of Medicine for their assistance in performing SNP arrays, and the Molecular Cytogenetics Core at MSKCC for Tel-FISH. J.T.H. is supported by a Research Scholars Grant, RSG-16-179-01-DMC, from the American Cancer Society. Support for this work also came from the Sontag Foundation (J.T.H.), the Sidney Kimmel Foundation (J.T.H.), and Cycle for Survival (J.T.H.). We acknowledge support from two NIH/NCI Cancer Center Support Grants (CCSGs) for MDACC (P30 CA016672) and MSKCC (P30 CA08748).

Author contributions: Conceptualization and design, Y.W., T.A.C. and J.T.H.; Development and methodology, Y.W., T.A.C. and J.T.H.; Acquisition of data, Y.W., W.H.W., R.S., and C.D.; Analysis and interpretation of data, Y.W., K.K., T.A.C., and J.T.H.; Writing, review, and/or revision of the manuscript, Y.W., K.K., T.A.C., and J.T.H.; Administrative, technical, or material support, G.J.R., K.K., E.P.S., T.A.C., and J.T.H.; Study supervision, T.A.C., and J.T.H.

References

1. Omuro, A. & DeAngelis, L.M. Glioblastoma and other malignant gliomas: a clinical review. *JAMA* **310**, 1842-50 (2013).
2. Brat, D.J. *et al.* Comprehensive, Integrative Genomic Analysis of Diffuse Lower-Grade Gliomas. *N Engl J Med* **372**, 2481-98 (2015).
3. Jiao, Y. *et al.* Frequent ATRX, CIC, FUBP1 and IDH1 mutations refine the classification of malignant gliomas. *Oncotarget* **3**, 709-22 (2012).
4. Schwartzentruber, J. *et al.* Driver mutations in histone H3.3 and chromatin remodelling genes in paediatric glioblastoma. *Nature* **482**, 226-31 (2012).
5. Gibbons, R.J. & Higgs, D.R. Molecular-clinical spectrum of the ATR-X syndrome. *Am J Med Genet* **97**, 204-12 (2000).
6. Drane, P., Ouararhni, K., Depaux, A., Shuaib, M. & Hamiche, A. The death-associated protein DAXX is a novel histone chaperone involved in the replication-independent deposition of H3.3. *Genes Dev* **24**, 1253-65 (2010).
7. Lewis, P.W., Elsaesser, S.J., Noh, K.M., Stadler, S.C. & Allis, C.D. Daxx is an H3.3-specific histone chaperone and cooperates with ATRX in replication-independent chromatin assembly at telomeres. *Proc Natl Acad Sci U S A* **107**, 14075-80 (2010).
8. Wong, L.H. *et al.* ATRX interacts with H3.3 in maintaining telomere structural integrity in pluripotent embryonic stem cells. *Genome Res* **20**, 351-60 (2010).
9. He, Q. *et al.* The Daxx/Atrx Complex Protects Tandem Repetitive Elements during DNA Hypomethylation by Promoting H3K9 Trimethylation. *Cell Stem Cell* **17**, 273-86 (2015).
10. Ratnakumar, K. *et al.* ATRX-mediated chromatin association of histone variant macroH2A1 regulates alpha-globin expression. *Genes Dev* **26**, 433-8 (2012).

524 11. Sarma, K. *et al.* ATRX Directs Binding of PRC2 to Xist RNA and Polycomb
525 Targets. *Cell* **159**, 869-83 (2014).
526 12. Voon, H.P. *et al.* ATRX Plays a Key Role in Maintaining Silencing at Interstitial
527 Heterochromatic Loci and Imprinted Genes. *Cell Rep* **11**, 405-18 (2015).
528 13. Clynes, D. *et al.* Suppression of the alternative lengthening of telomere pathway
529 by the chromatin remodelling factor ATRX. *Nat Commun* **6**, 7538 (2015).
530 14. Heaphy, C.M. *et al.* Altered telomeres in tumors with ATRX and DAXX mutations.
531 *Science* **333**, 425 (2011).
532 15. Baumann, C., Viveiros, M.M. & De La Fuente, R. Loss of maternal ATRX results
533 in centromere instability and aneuploidy in the mammalian oocyte and pre-
534 implantation embryo. *PLoS Genet* **6**(2010).
535 16. Clynes, D. *et al.* ATRX dysfunction induces replication defects in primary mouse
536 cells. *PLoS One* **9**, e92915 (2014).
537 17. Koschmann, C. *et al.* ATRX loss promotes tumor growth and impairs
538 nonhomologous end joining DNA repair in glioma. *Sci Transl Med* **8**, 328ra28
539 (2016).
540 18. Leung, J.W. *et al.* Alpha thalassemia/mental retardation syndrome X-linked gene
541 product ATRX is required for proper replication restart and cellular resistance to
542 replication stress. *J Biol Chem* **288**, 6342-50 (2013).
543 19. Lovejoy, C.A. *et al.* Loss of ATRX, Genome Instability, and an Altered DNA
544 Damage Response Are Hallmarks of the Alternative Lengthening of Telomeres
545 Pathway. *PLoS Genet* **8**, e1002772 (2012).
546 20. Ritchie, K. *et al.* Loss of ATRX leads to chromosome cohesion and congression
547 defects. *J Cell Biol* **180**, 315-24 (2008).
548 21. Law, M.J. *et al.* ATR-X syndrome protein targets tandem repeats and influences
549 allele-specific expression in a size-dependent manner. *Cell* **143**, 367-78 (2010).

22. Clynes, D., Higgs, D.R. & Gibbons, R.J. The chromatin remodeller ATRX: a repeat offender in human disease. *Trends Biochem Sci* **38**, 461-6 (2013).

23. Paeschke, K., Capra, J.A. & Zakian, V.A. DNA replication through G-quadruplex motifs is promoted by the Saccharomyces cerevisiae Pif1 DNA helicase. *Cell* **145**, 678-91 (2011).

24. Rodriguez, R. *et al.* Small-molecule-induced DNA damage identifies alternative DNA structures in human genes. *Nat Chem Biol* **8**, 301-10 (2012).

25. Watson, L.A. *et al.* Atrx deficiency induces telomere dysfunction, endocrine defects, and reduced life span. *J Clin Invest* **123**, 2049-63 (2013).

26. Turcan, S. *et al.* IDH1 mutation is sufficient to establish the glioma hypermethylator phenotype. *Nature* **483**, 479-83 (2012).

27. Turcan, S. *et al.* Mutant-IDH1-dependent chromatin state reprogramming, reversibility, and persistence. *Nat Genet* **50**, 62-72 (2018).

28. Ohba, S. *et al.* Mutant IDH1 Expression Drives TERT Promoter Reactivation as Part of the Cellular Transformation Process. *Cancer Res* **76**, 6680-6689 (2016).

29. Johannessen, T.A. *et al.* Rapid Conversion of Mutant IDH1 from Driver to Passenger in a Model of Human Gliomagenesis. *Mol Cancer Res* **14**, 976-983 (2016).

30. Ohba, S., Mukherjee, J., See, W.L. & Pieper, R.O. Mutant IDH1-driven cellular transformation increases RAD51-mediated homologous recombination and temozolomide resistance. *Cancer Res* **74**, 4836-44 (2014).

31. Cawthon, R.M. Telomere measurement by quantitative PCR. *Nucleic Acids Res* **30**, e47 (2002).

32. Hansel-Hertsch, R. *et al.* G-quadruplex structures mark human regulatory chromatin. *Nat Genet* **48**, 1267-72 (2016).

575 33. Pan, Y.F. *et al.* Regulation of estrogen receptor-mediated long range
576 transcription via evolutionarily conserved distal response elements. *J Biol Chem*
577 **283**, 32977-88 (2008).
578 34. Rhodes, D. & Lipps, H.J. G-quadruplexes and their regulatory roles in biology.
579 *Nucleic Acids Research* **43**, 8627-8637 (2015).
580 35. Drygin, D. *et al.* Anticancer activity of CX-3543: a direct inhibitor of rRNA
581 biogenesis. *Cancer Res* **69**, 7653-61 (2009).
582 36. Balasubramanian, S., Hurley, L.H. & Neidle, S. Targeting G-quadruplexes in
583 gene promoters: a novel anticancer strategy? *Nat Rev Drug Discov* **10**, 261-75
584 (2011).
585 37. Borodovsky, A. *et al.* A model of a patient-derived IDH1 mutant anaplastic
586 astrocytoma with alternative lengthening of telomeres. *J Neurooncol* **121**, 479-87
587 (2015).
588 38. Danussi, C. *et al.* Atrx inactivation drives disease-defining phenotypes in glioma
589 cells of origin through global epigenomic remodeling. *Nat Commun* **9**, 1057
590 (2018).
591 39. Rizzo, A. *et al.* Stabilization of quadruplex DNA perturbs telomere replication
592 leading to the activation of an ATR-dependent ATM signaling pathway. *Nucleic*
593 *Acids Res* **37**, 5353-64 (2009).
594 40. Berube, N.G. *et al.* The chromatin-remodeling protein ATRX is critical for
595 neuronal survival during corticogenesis. *J Clin Invest* **115**, 258-67 (2005).
596 41. Huh, M.S. *et al.* Stalled replication forks within heterochromatin require ATRX for
597 protection. *Cell Death Dis* **7**, e2220 (2016).
598 42. Branzei, D. & Foiani, M. The checkpoint response to replication stress. *DNA*
599 *Repair (Amst)* **8**, 1038-46 (2009).

43. Petermann, E. & Helleday, T. Pathways of mammalian replication fork restart. *Nat Rev Mol Cell Biol* **11**, 683-7 (2010).

44. Pflumm, M.F. The role of DNA replication in chromosome condensation. *Bioessays* **24**, 411-8 (2002).

45. De, S. & Michor, F. DNA secondary structures and epigenetic determinants of cancer genome evolution. *Nat Struct Mol Biol* **18**, 950-5 (2011).

46. von Deimling, A. *et al.* Diffuse astrocytoma, IDH-mutant. in *WHO classification of tumours of the central nervous system* (eds. Louis, D.N., Ohgaki, H., Wiestler, O.D. & Cavenee, W.K.) 18-23 (International agency for research on cancer (IARC), Lyon, 2016).

47. Helleday, T. The underlying mechanism for the PARP and BRCA synthetic lethality: clearing up the misunderstandings. *Mol Oncol* **5**, 387-93 (2011).

48. Laperriere, N., Zuraw, L. & Cairncross, G. Radiotherapy for newly diagnosed malignant glioma in adults: a systematic review. *Radiother Oncol* **64**, 259-73 (2002).

49. Walker, M.D. *et al.* Evaluation of BCNU and/or radiotherapy in the treatment of anaplastic gliomas. A cooperative clinical trial. *J Neurosurg* **49**, 333-43 (1978).

50. Walker, M.D. *et al.* Randomized comparisons of radiotherapy and nitrosoureas for the treatment of malignant glioma after surgery. *N Engl J Med* **303**, 1323-9 (1980).

51. Wiestler, B. *et al.* ATRX loss refines the classification of anaplastic gliomas and identifies a subgroup of IDH mutant astrocytic tumors with better prognosis. *Acta Neuropathol* **126**, 443-51 (2013).

52. Cairncross, J.G. *et al.* Benefit from procarbazine, lomustine, and vincristine in oligodendroglial tumors is associated with mutation of IDH. *J Clin Oncol* **32**, 783-90 (2014).

53. Sulkowski, P.L. *et al.* 2-Hydroxyglutarate produced by neomorphic IDH mutations suppresses homologous recombination and induces PARP inhibitor sensitivity. *Science Translational Medicine* **9**(2017).

54. Molenaar, R.J. *et al.* IDH1/2 mutations sensitize acute myeloid leukemia to PARP inhibition and this is reversed by IDH1/2-mutant inhibitors. *Clin Cancer Res* (2018).

55. Lu, Y.X. *et al.* Chemosensitivity of IDH1-Mutated Gliomas Due to an Impairment in PARP1-Mediated DNA Repair. *Cancer Research* **77**, 1709-1718 (2017).

56. Xu, H. *et al.* CX-5461 is a DNA G-quadruplex stabilizer with selective lethality in BRCA1/2 deficient tumours. *Nat Commun* **8**, 14432 (2017).

57. Zheng, X.H. *et al.* A Cisplatin Derivative Tetra-Pt(bpy) as an Oncotherapeutic Agent for Targeting ALT Cancer. *J Natl Cancer Inst* **109**(2017).

58. Sonoda, Y. *et al.* Formation of intracranial tumors by genetically modified human astrocytes defines four pathways critical in the development of human anaplastic astrocytoma. *Cancer Research* **61**, 4956-4960 (2001).

59. Rohle, D. *et al.* An inhibitor of mutant IDH1 delays growth and promotes differentiation of glioma cells. *Science* **340**, 626-30 (2013).

60. Henderson, A. *et al.* Detection of G-quadruplex DNA in mammalian cells. *Nucleic Acids Research* **42**, 860-869 (2014).

61. Lam, E.Y., Beraldi, D., Tannahill, D. & Balasubramanian, S. G-quadruplex structures are stable and detectable in human genomic DNA. *Nat Commun* **4**, 1796 (2013).

62. Fernando, H., Rodriguez, R. & Balasubramanian, S. Selective recognition of a DNA G-quadruplex by an engineered antibody. *Biochemistry* **47**, 9365-71 (2008).

63. Korn, J.M. *et al.* Integrated genotype calling and association analysis of SNPs, common copy number polymorphisms and rare CNVs. *Nat Genet* **40**, 1253-60 (2008).

64. Venkatraman, E.S. & Olshen, A.B. A faster circular binary segmentation algorithm for the analysis of array CGH data. *Bioinformatics* **23**, 657-63 (2007).

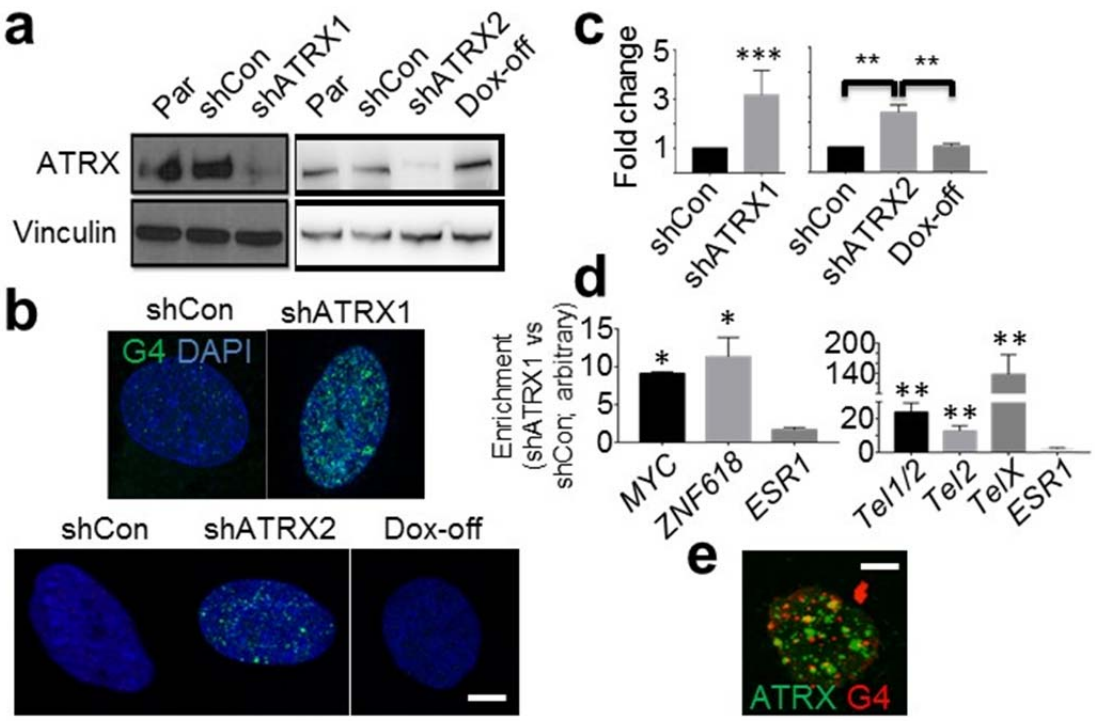

Figures and Legends:

FIG. 1: ATRX deficiency promotes G4 formation a: Western blots for ATRX in parental (Par), shControl (shCon) and shATRX NHA (Vinculin loading control). Left panel shows stable NHA lines (shATRX1) and right panel shows the inducible lines post Doxycycline induction (shATRX2) and withdrawal (Dox-off). **b:** Immunofluorescent staining of G4 in the stable (upper panel) and inducible (lower panel) NHA lines (DAPI counterstain). **c:** Quantified relative G4 signal intensity. **d:** G4-containing DNA fragments from shCon and shATRX1 NHAs were pulled down from sheared genomic DNA with purified hf2 antibodies. Recovered DNA was subjected to real-time PCR for telomeric sequences or G4-rich promoter regions of *MYC and ZNF618* (*ESR1* used as negative control). Graphs show enrichment over GAPDH scaled to shCon levels. **e:** ATRX and G4 immunofluorescence in parental NHAs showing no significant colocalization.

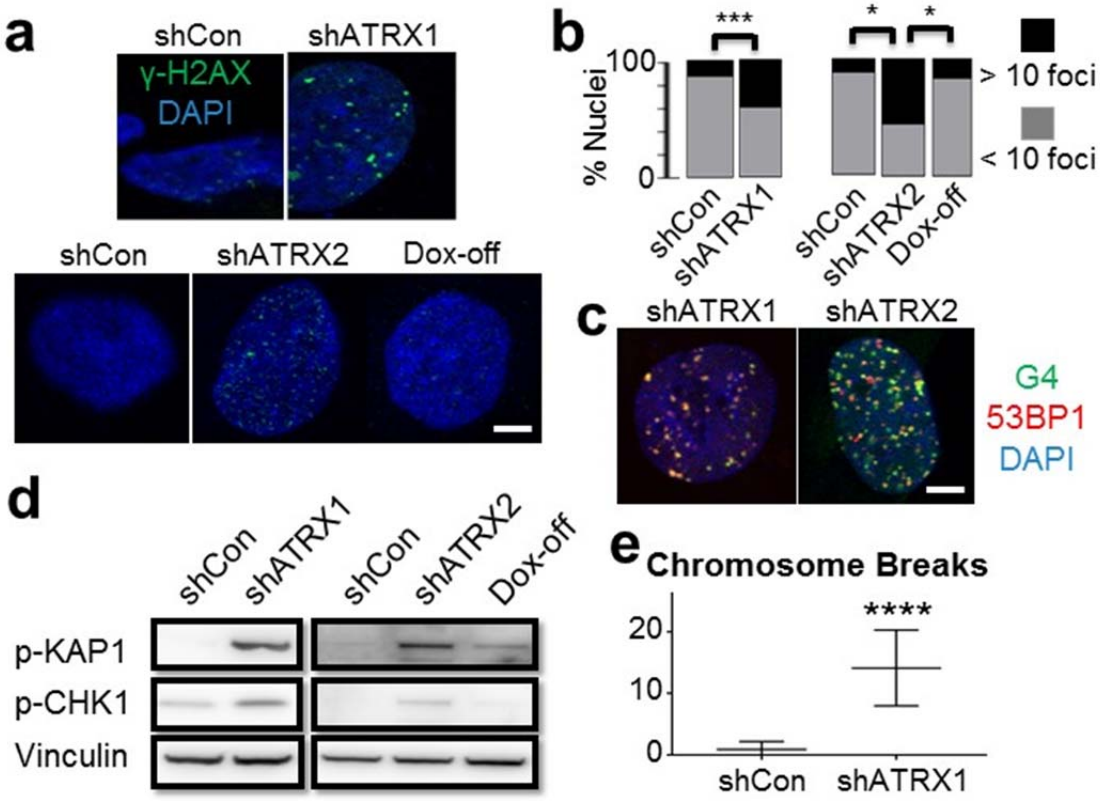

FIG. 2: ATRX deficiency promotes replication stress, DNA damage, and chromosome breakage. **a:** γ-H2AX immunofluorescence in stable (upper panel) and inducible (lower panel) NHAs (DAPI counterstain). **b:** Quantified percentage of cells with >10 immunopositive γ-H2AX foci . **c:** NHAs with ATRX knock down were double stained for G4 and 53BP1, showing extensive colocalization. **d:** Western blots of p-KAP1 and p-CHK1 show activation of replication stress arising with ATRX knockdown. **e:** ATRX deficient NHAs (shATRX1, passage 15) showed significantly increased chromosome breaks by cytogenetic analysis.

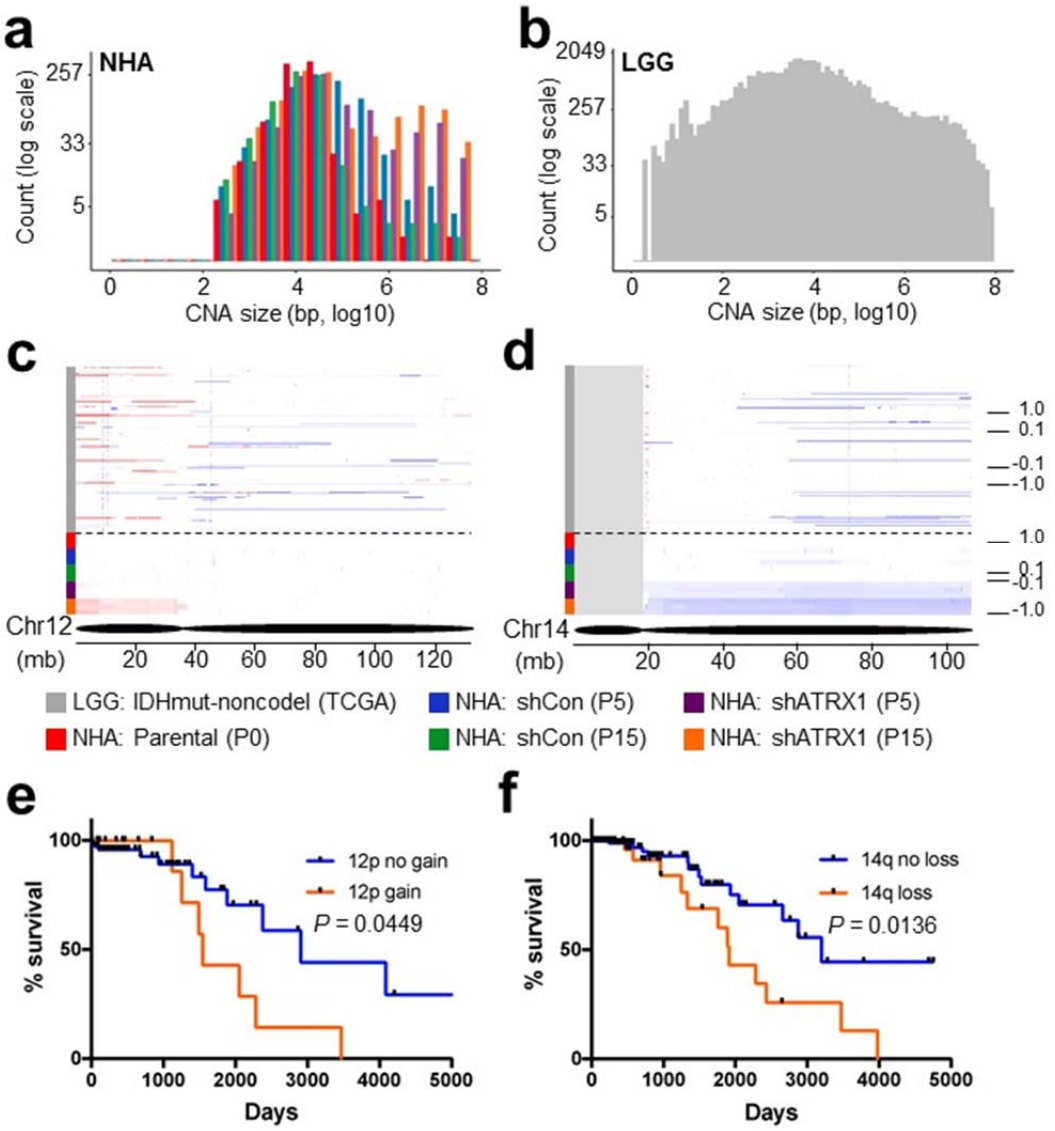

680

681 **FIG. 3: ATRX deficiency induces clinically relevant copy number alterations. a:**
682 Size distribution of CNAs in parental (P0), shCon (P5 and P15) and shATRX1 (P5 and
683 P15) NHAs. In ATRX knockdown cells, large CNAs (>1 Mb) arise over passage number.
684 **b:** Size distribution of CNAs in IDHmut-noncodel gliomas (TCGA)[2]. **c-d:** IGV plots for
685 chromosome 12 (c) and 14 (d) comparing CNA regions in IDHmut-nocodel gliomas
686 (above dotted line) to NHAs (below dotted line). **e-f:** Kaplan Meier curves for IDHmut-
687 noncodel glioma patients with or without either 12p gain or 14q loss, showing significant
688 differences in overall survival.

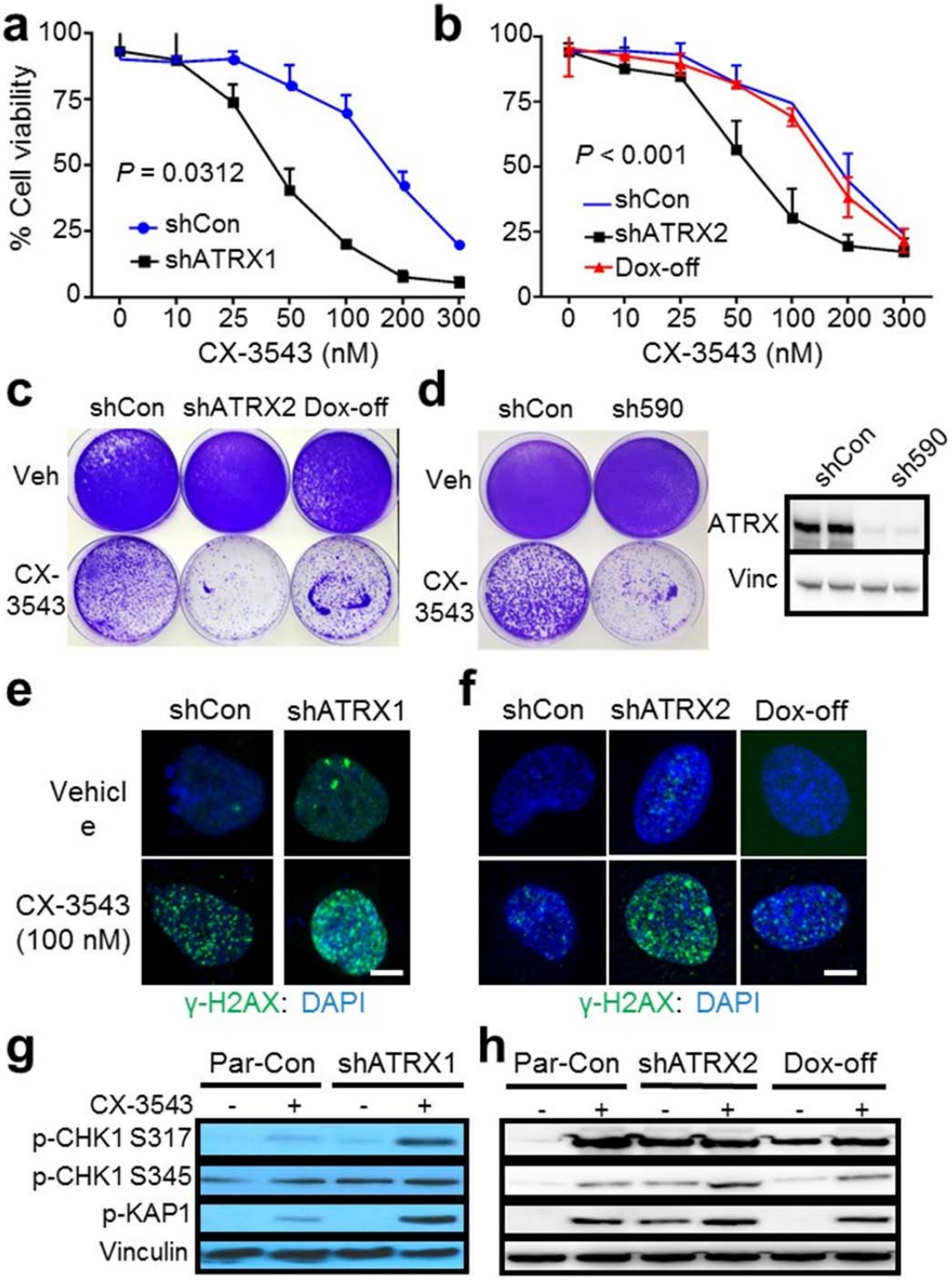

FIG. 4: ATRX-deficient NHAs are selectively sensitive to CX-3543. a-b: Cell viability (CellTiter-Glo) of stable (a) and inducible (b) shCon and shATRX NHAs treated with CX-3543 from 0-300nM. **c:** Clonogenic assay of inducible shATRX2 NHAs demonstrates

enhanced and reversible sensitivity to CX-3543 (50 nM) with ATRX deficiency. **d:** Clonogenic assay of TS 543 with (sh590) and without (shCon) ATRX knockdown demonstrates enhanced sensitivity to CX-3543 (50 nM) with ATRX deficiency; western blot confirms robust ATRX knockdown (Vinculin control, duplicate loading). **e-f:** γ-H2AX immunofluorescence showing in stable (c) and inducible (d) shATRX NHAs showing increased DNA damage with CX-3543 treatment (100 nM), particularly in the setting of ATRX knockdown. **g-h:** Western blots showing increased phosphorylation of replication stress pathway constituents (CHK1 and KAP1) in stable (e) and inducible (f) shATRX NHAs following CX-3543 treatment (100 nM).

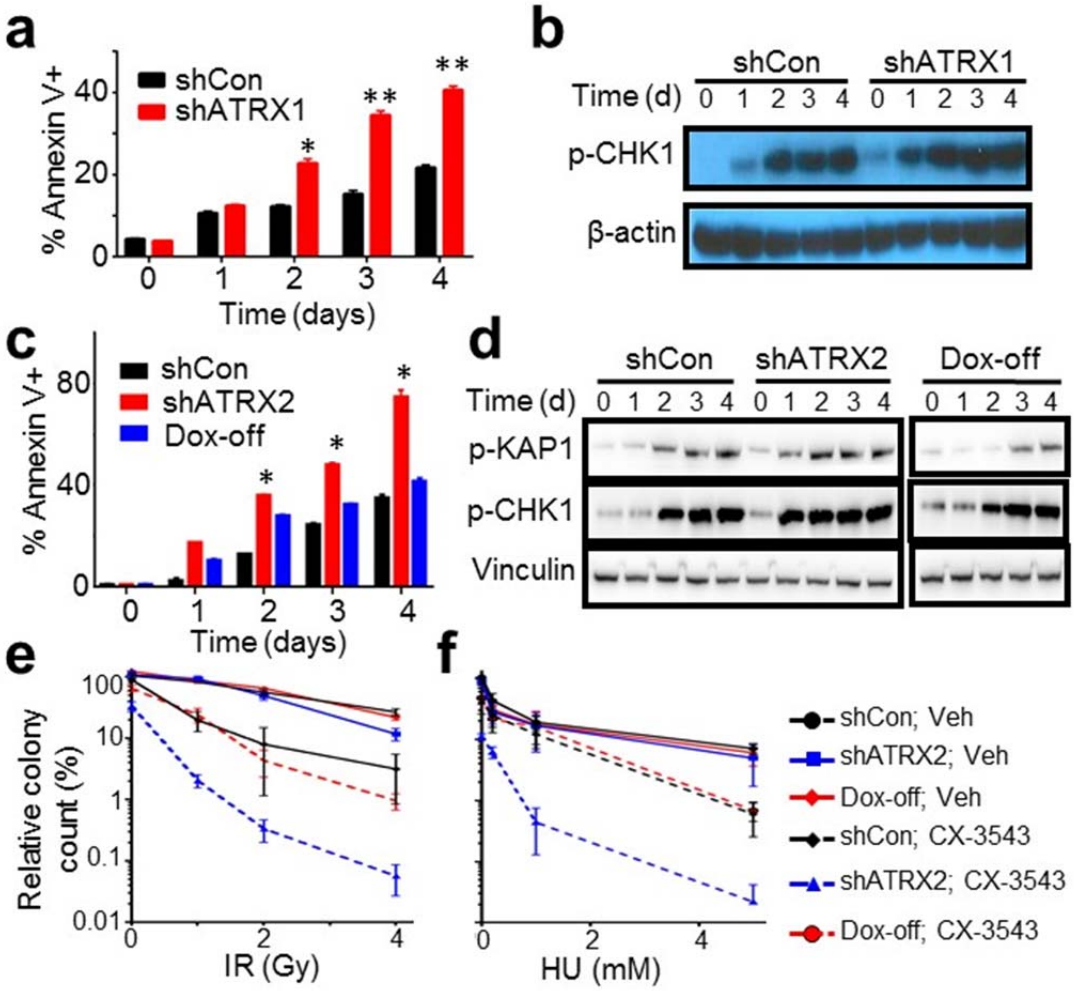

FIG. 5: CX-3543 selectively promotes apoptosis and synergizes with DNA-damaging therapies in ATRX-deficient NHAs. a-b: : Time course study in shCon and shATRX1 NHAs treated with 100 nM CX-3543 showing parallel kinetics of apoptosis (Annexin V positivity; a) and p-CHK1/p-KAP1 levels by western blot (b). **c-d:** Analgous time course study in inducible shATRX2 cells documenting p-CHK1 an p-KAP1 levels (d) by western blot and Annexin V positivity (c) over time. **e-f:** Soft agar colony counts for NHAs treated with either vehicle control (Veh) or 50 nM CX-3543 and either increasing doses of IR (a) or HU (b). Colony counts measured at 21 days scaled to that of shCon, Veh NHAs.

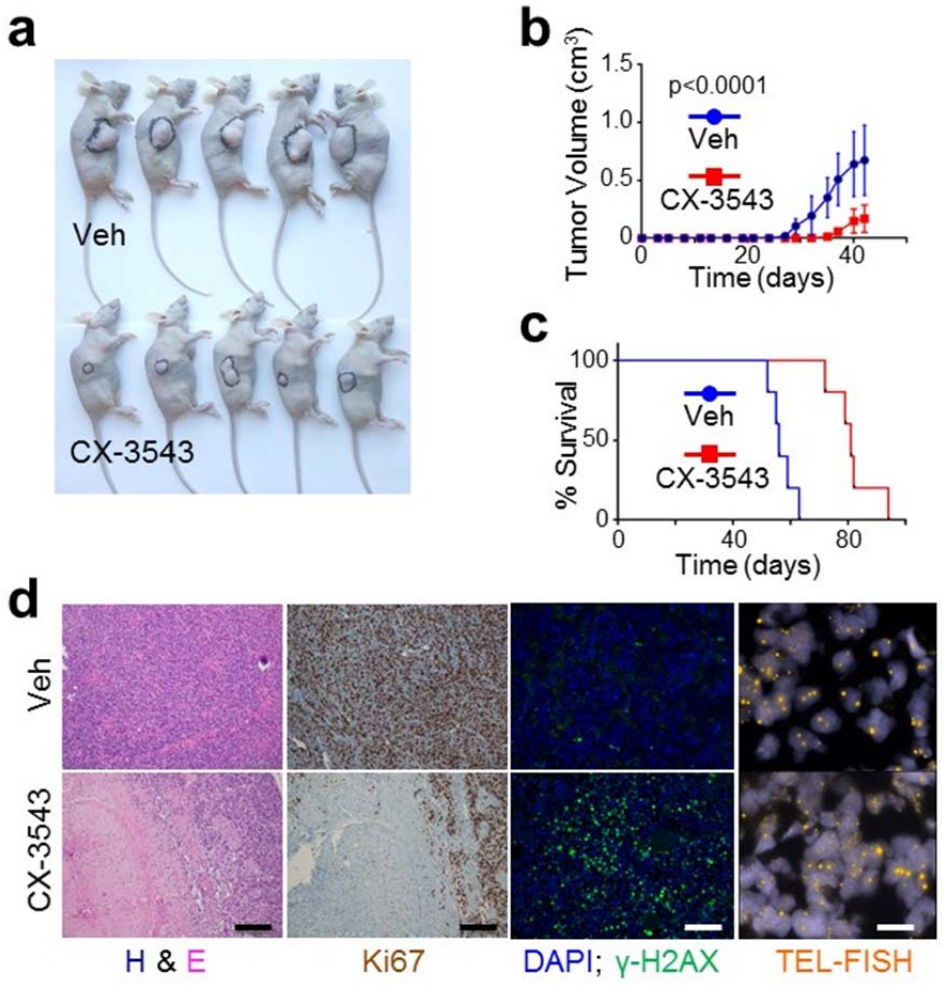

FIG. 6: CX-3543 markedly slows the growth of ATRX-mutant glioma xenografts *in vivo*. a: representative image of mice bearing JHH-273 xenografts following treatment with either vehicle (veh) or 12.5 mg/kg CX-3543 for 42 days. **b:** Average xenograft volume over time in 10 mice randomized (5 and 5) into 2 groups, receiving either 12.5 mg/kg CX-3543 or vehicle control (veh). **c:** Kaplan-Meier analysis of survival In a separate cohort of 10 mice randomized (5 and 5) into 2 groups, receiving either 12.5 mg/kg CX-3543 or vehicle control (Veh). **d:** Representative H&E-stained, immunostained (Ki67 and γ-H2AX), and TEL-FISH stained sections of xenografts from vehicle (Veh) and CX-3543-treated mice. CX-3543-treated tumors showed decreased cellularity, decreased proliferative activity, and increased DNA damage.

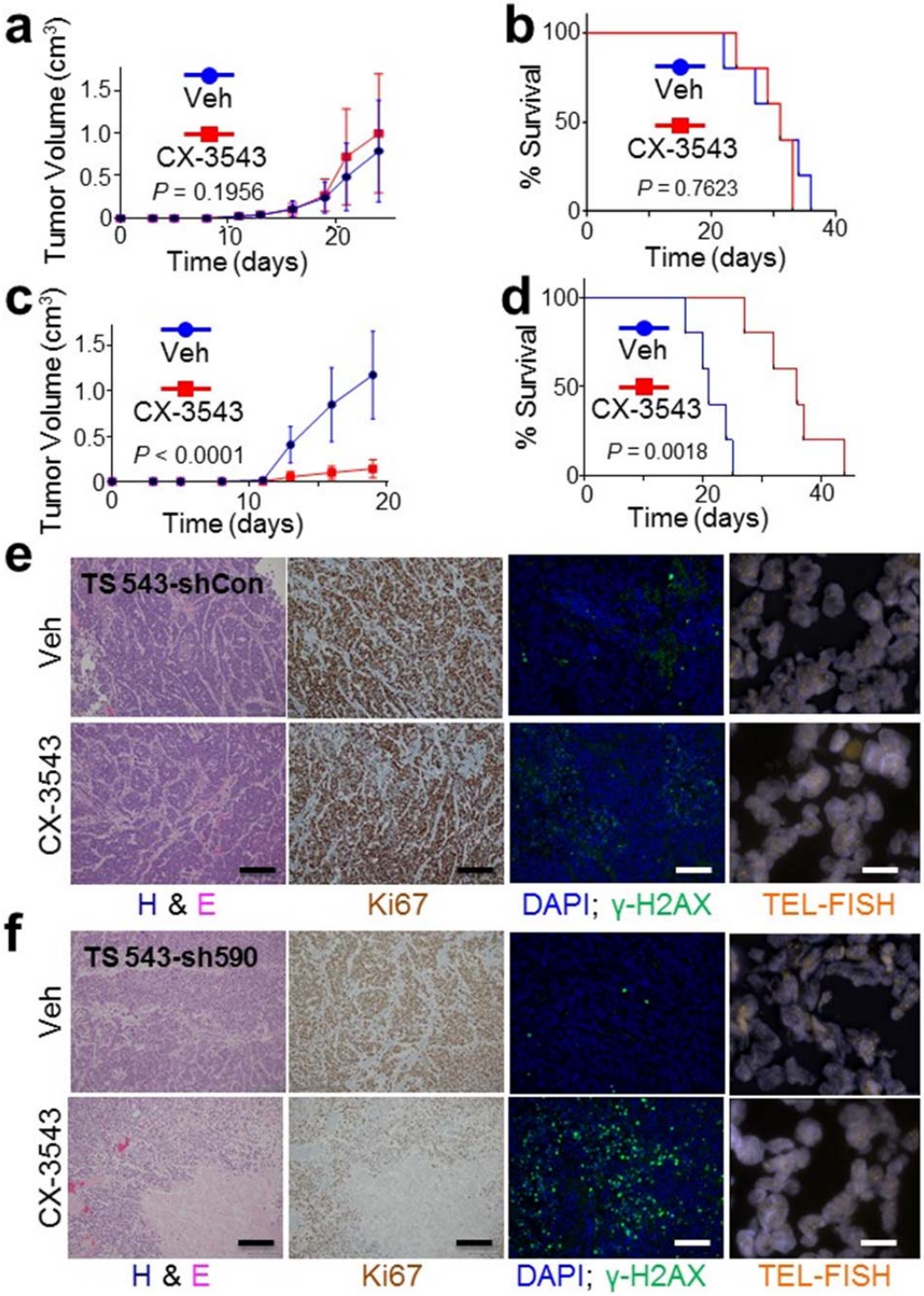

FIG. 7: Efficacy of CX-3543 *in vivo* is dependent on ATRX deficiency. a: TS 543 (ATRX intact) xenografts exhibited similar rates of growth when treated with either vehicle control (Veh, N=3) or 12.5 mg/kg CX-3543 (N=3) as reflected by tumor volume over time. **b:** Kaplan-Meier analysis of survival In a separate cohort of 10 mice

729 randomized (5 and 5) into 2 groups, receiving either 12.5 mg/kg CX-3543 or vehicle
730 control (Veh). **c:** ATRX knockdown in TS 543 cells (sh590) restored the sensitivity of
731 xenografts to CX-3543 treatment as shown by tumor volume over time in 10 mice
732 randomized (5 and 5) into 2 groups, receiving either 12.5 mg/kg CX-3543 or vehicle
733 control (Veh). **d:** Kaplan-Meier analysis of survival In a separate cohort of 10 mice
734 randomized (5 and 5) into 2 groups, receiving either 12.5 mg/kg CX-3543 or vehicle
735 control (Veh). **e-f:** Representative H&E-stained, immunostained (Ki67 and γ-H2AX), and
736 TEL-FISH stained sections of xenografts from vehicle (Veh) and CX-3543-treated mice
737 harboring either TS 543-shCon (a) or TS 543-sh590 (b) xenografts. CX-3543-associated
738 histopathological effects were limited to TS 543-sh590 xenografts. Evidence of ALT was
739 not seen in either GSC line.
740